Hindawi Publishing Corporation
Journal of Sensors
Volume 2014, Article ID 739161, 9 pages
http://dx.doi.org/10.1155/2014/739161

*Review Article*

# Contactless Inductive Flow Tomography: Brief History and Recent Developments in Its Application to Continuous Casting

**Matthias Ratajczak, Thomas Gundrum, Frank Stefani, and Thomas Wondrak**

*Helmholtz-Zentrum Dresden-Rossendorf, P.O. Box 510119, 01314 Dresden, Germany*

Correspondence should be addressed to Frank Stefani; f.stefani@hzdr.de

Received 13 June 2014; Accepted 7 August 2014; Published 17 September 2014

Academic Editor: Mohd Hafiz Fazalul Rahiman

Copyright © 2014 Matthias Ratajczak et al. This is an open access article distributed under the Creative Commons Attribution License, which permits unrestricted use, distribution, and reproduction in any medium, provided the original work is properly cited.

The contactless inductive flow tomography (CIFT) aims at reconstructing the velocity field of electrically conducting fluids, with special focus on applications in metallurgy and crystal growth technologies. The method relies on the induction of secondary magnetic fields if the moving fluid is exposed to a primary magnetic field. The theoretical foundation of the method is delineated, and some early experiments on the reconstruction of the three-dimensional flow in a cylinder are sketched. Then, the recent efforts to apply CIFT to various model problems in connection with the continuous casting of steel are summarized.

## 1. Introduction

In many metallurgical and crystal growth applications it would be highly desirable to monitor the velocity field of the metal or semiconductor melt. The opaqueness of those melts prevents the use of optical measurement techniques, such as laser Doppler anemometry (LDA) or particle image velocimetry (PIV). Nonoptical flow measurement techniques, using ultrasonic beams or special probes (pressure probes and potential probes), face problems, too, if the melts are hot and/or chemically aggressive. A nonintrusive or, better, a completely contactless method for flow reconstruction would be most helpful in these cases.

The contactless inductive flow tomography (CIFT) [1] promises to provide at least a rough picture of the flow by applying primary magnetic fields to the melt and by measuring the flow induced (secondary) magnetic field perturbation outside the fluid volume. The inverse problem of determining the flow velocity from those induced magnetic fields is, in some sense, quite similar to the corresponding problem in magnetoencephalography (MEG) where electric currents in the human brain are to be identified [2]. A significant difference between CIFT and MEG is, however, that the wanted velocity field is divergence-free which gives an additional constraint for the inverse problem. The still remaining nonuniqueness can be overcome by using appropriate regularization methods, such as Tikhonov regularization and the L-curve technique [3], in which a certain quadratic functional of the velocity, for example, the kinetic energy or the squared curvature, is additionally minimized.

A further difference to MEG is the fact that the primary magnetic field can be applied in various directions. As long as the typical time for velocity changes is larger than the switching times for the different applied fields, this allows collecting more information about (basically) the same velocity field which further reduces the uncertainties.

Despite some similarities in the measurement concept, CIFT must be distinguished clearly from the magnetic induction tomography, sometimes also called mutual inductance tomography (MIT) [4, 5]. While the former relies on induced currents due to the interaction of a moving liquid with an applied DC or relatively low frequency AC magnetic field, the latter aims at reconstructing conductivity distributions in a body by utilizing the eddy currents which are induced in a relatively high frequency AC magnetic field.

With the intention to give a self-contained introduction to CIFT, we start by reiterating the basic mathematics for the forward and the inverse problem as it had been developed some fifteen years ago [6–8]. In Section 3, we summarize the results of first test experiment which had shown the applicability of CIFT for the reconstruction of three-dimensional velocity fields [1]. With view on the later application to the continuous casting of steel [9–13], we focus then on the reduction of CIFT to the (essentially) two-dimensional geometry of slab-casting for which some experimental results are illustrated. In this context we also present some new results evidencing the feasibility of CIFT in the presence of a strong magnetic brake field. The paper concludes with an outlook on future methodological developments and possible industrial implementations of CIFT.

## 2. Mathematical Foundation

In this section we give a short outline of the theory of CIFT. For more details, in particular concerning the nonuniqueness problem of the ill-posed inverse problem, we refer the reader to the previous papers [6–8].

We consider an electrically conductive fluid with a velocity field **v,** that is, for the moment, assumed to be steady. Imagine this moving fluid to be exposed to a stationary magnetic field **B**. Then, according to Ohm's law in moving conductors, the current density

$$\mathbf{j} = \sigma\left(\mathbf{v} \times \mathbf{B} - \nabla\varphi\right) \tag{1}$$

is induced, where $\sigma$ is the electrical conductivity of the fluid and $\varphi$ denotes the electric scalar potential. According to Biot-Savart's law [8, 14], this current density **j** induces now a secondary magnetic field **b** at a given position **r**:

$$\begin{aligned}\mathbf{b}(\mathbf{r}) = {} & \frac{\mu_0\sigma}{4\pi}\iiint_V \left[\mathbf{v}\left(\mathbf{r}'\right) \times \mathbf{B}\left(\mathbf{r}'\right)\right] \times \frac{\mathbf{r}-\mathbf{r}'}{\left|\mathbf{r}-\mathbf{r}'\right|^3} dV' \\ & - \frac{\mu_0\sigma}{4\pi}\oiint_S \varphi\left(\mathbf{s}'\right)\mathbf{n}\left(\mathbf{s}'\right) \times \frac{\left(\mathbf{r}-\mathbf{s}'\right)}{\left|\mathbf{r}-\mathbf{s}'\right|^3} dS'.\end{aligned} \tag{2}$$

In the volume integral, $dV'$ denotes the volume element and $\mathbf{r}'$ the position vector in the volume. In the surface integral, $dS'$ denotes a surface element and $\mathbf{n}(\mathbf{s}')$ denotes the normal vector of the surface at the position $\mathbf{s}'$.

It is essential to not forget the second term on the r.h.s. of (2) (early attempts [15, 16] to develop a magnetic flow tomography were flawed by this omission). Only in very special cases, for example, if a simple poloidal flow is exposed to an axial magnetic field so that the induced current flows only in azimuthal direction, the second term is zero. If, however, a purely azimuthal flow is exposed to an axial field, the second term completely cancels out the first term.

Exploiting the fact that **j** is divergence-free, one can derive from (1) a Poisson equation for the electric potential:

$$\Delta\varphi = \nabla \cdot (\mathbf{v} \times \mathbf{B}). \tag{3}$$

According to Green's theorem, the solution of this Poisson equation fulfills the boundary integral equation

$$\begin{aligned}\varphi(\mathbf{s}) = {} & \frac{1}{2\pi}\iiint_V \left[\mathbf{v}\left(\mathbf{r}'\right) \times \mathbf{B}\left(\mathbf{r}'\right)\right] \cdot \frac{\mathbf{s}-\mathbf{r}'}{\left|\mathbf{s}-\mathbf{r}'\right|^3} dV' \\ & - \frac{1}{2\pi}\oiint_S \varphi\left(\mathbf{s}'\right)\mathbf{n}\left(\mathbf{s}'\right) \cdot \frac{\left(\mathbf{s}-\mathbf{s}'\right)}{\left|\mathbf{s}-\mathbf{s}'\right|^3} dS',\end{aligned} \tag{4}$$

if insulating boundaries are assumed.

In general, the total magnetic field **B** under the integrals of (2) and (4) is the sum of an externally applied primary magnetic field $\mathbf{B}_0$ and the induced secondary magnetic field **b** itself. The ratio between **b** and $\mathbf{B}_0$ is proportional to the magnetic Reynolds number, defined as

$$R_m = \mu_0\sigma l v, \tag{5}$$

with $l$ and $v$ denoting characteristic length and velocity scales of the fluid, respectively. For large values of $R_m$ and suitable flow topologies, it is possible to achieve self-excitation of a magnetic field. In this case, one can obtain solutions of (2) and (4) even for $\mathbf{B}_0 = 0$. Such homogeneous dynamos have indeed been studied [14, 17] by solving the integral equation system (2) and (4).

However, in most industrial applications $R_m$ is smaller than 1. To take continuous casting of steel as a typical example, with a mould width of 1 m, a typical flow velocity of 0.1 m/s, and a conductivity of the liquid steel of $7 \cdot 10^5$ S/m, we arrive approximately at $R_m = 0.1$. In such cases, **B** can be replaced by $\mathbf{B}_0$ under the integrals in (2) and (4). In this approximation, we get a linear inverse problem for the determination of the velocity field **v** from the induced magnetic field **b** measured in the exterior of the fluid. Of course, the unknown electric potential at the fluid boundary must not be neglected and has to be treated in due manner.

We assume now $K$ different external magnetic fields $\mathbf{B}_{0,k}$ to be applied to the fluid. Suppose, for each $\mathbf{B}_{0,k}$, all measured induced magnetic field components to be collected into an $n_b$-dimensional vector with the entries $b_i^{B_{0,k}}$. Accordingly, the discretized electric potential at the surface $S$ is collected into an $n_\varphi$-dimensional vector with the entries $\varphi_j^{B_{0,k}}$, and the desired velocity **v** in the volume $V$ is discretized as an $n_v$-dimensional vector with the entries $v_l$. Then, (2) and (4) can formally be written in the following matrix form:

$$b_i^{B_{0,k}} = R_{il}^{B_{0,k}} v_l + S_{ij}\varphi_j^{B_{0,k}}, \tag{6}$$

$$\varphi_j^{B_{0,k}} = T_{jl}^{B_{0,k}} v_l + U_{jj'}\varphi_{j'}^{B_{0,k}}. \tag{7}$$

Note that only the matrices $\mathbf{R}^{B_{0,k}}$ and $\mathbf{T}^{B_{0,k}}$ depend on the applied magnetic field $\mathbf{B}_{0,k}$, whereas the matrices **S** and **U** depend on the geometry only.

A peculiarity of (7) is well known from magnetoencephalography (MEG) [2]. Actually, the matrix $(\mathbf{I} - \mathbf{U})$ is singular which indicates the fact that the electric potential is defined only up to an additional constant. This problem can be circumvented by using the so-called deflation method [2],

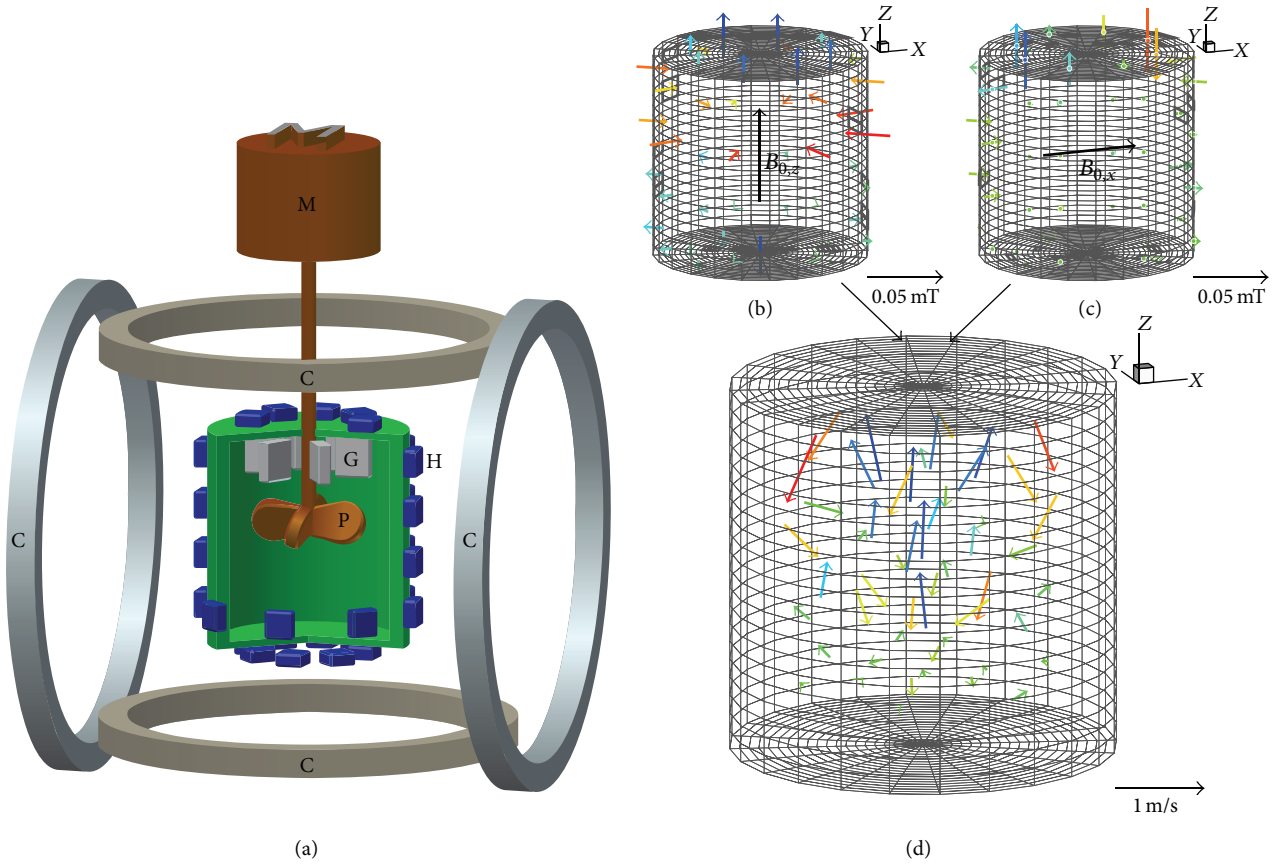


FIGURE 1: (a) Schematic sketch of the experiment for the validation of CIFT at a propeller driven 3D flow using GaInSn. M—motor, C—coils, P—propeller, G—guiding blades, and H—Hall sensors. (b) Measured induced field at 48 positions for upward pumping propeller for applied $B_{0,z}$. The arrows indicate the field component measured by the Hall sensors. (c) Same as (b), but for applied $B_{0,x}$. (d) Velocity field as reconstructed by CIFT from (b) and (c).

replacing $(\mathbf{I} - \mathbf{U})$ by the well-conditioned matrix $(\mathbf{I} - \mathbf{U})^{\text{defl}}$. Inserting the solution $\varphi$ of (deflated) equation (7) into (6) we end up with a single linear relationship between the desired velocity field and the measured magnetic field in the form

$$b_i^{B_{0,k}} = R_{il}^{B_{0,k}} v_l + S_{ij'} \left( (I - U)^{-1,\text{defl}} \right)_{j'j} T_{jl}^{B_{0,k}} v_l. \tag{8}$$

For further details of the numerical solution of this equation, in particular concerning the accurate computation of the boundary integrals, see [18].

We can now derive the velocity by solving the normal equations arising from the minimization of the following total functional of the velocity field:

$$F[\mathbf{v}] = \sum_{k=1}^{K} F_{B_{0,k}}[\mathbf{v}] + F_{\text{div}}[\mathbf{v}] + F_{\text{pen}}[\mathbf{v}] \tag{9}$$

with

$$\begin{aligned} F_{B_{0,k}}[\mathbf{v}] &= \frac{1}{\sigma_{B_{0,k}}^2} \sum_{i=1}^{n_b} \left\{ b_{i,\text{measured}}^{B_{0,k}} - b_{i,\text{modeled}}^{B_{0,k}}[\mathbf{v}] \right\}^2, \\ F_{\text{div}}[\mathbf{v}] &= \frac{1}{\sigma_{\text{div}}^2} \sum_{l=1}^{n_V} \Delta V_l (\nabla \cdot \mathbf{v})_l^2, \\ F_{\text{pen}}[\mathbf{v}] &= \frac{1}{\sigma_{\text{pen}}^2} \sum_{l=1}^{n_V} \Delta V_l \mathbf{v}_l^2, \end{aligned} \tag{10}$$

where $\Delta V_l$ denotes the volume of the element at the grid point $l$. The first sum over the functionals $F_{B_{0,k}}$ is the most essential one as it represents the mean squared residual deviation of the measured magnetic fields $b_{i,\text{measured}}^{B_{0,k}}$ from the fields $b_{i,\text{modeled}}^{B_{0,k}}$ modeled according to (8).

The functional $F_{\text{div}}[\mathbf{v}]$ enforces the velocity field to be solenoidal, and the last functional $F_{\text{pen}}[\mathbf{v}]$ is the regularization functional which tries to minimize the kinetic energy.

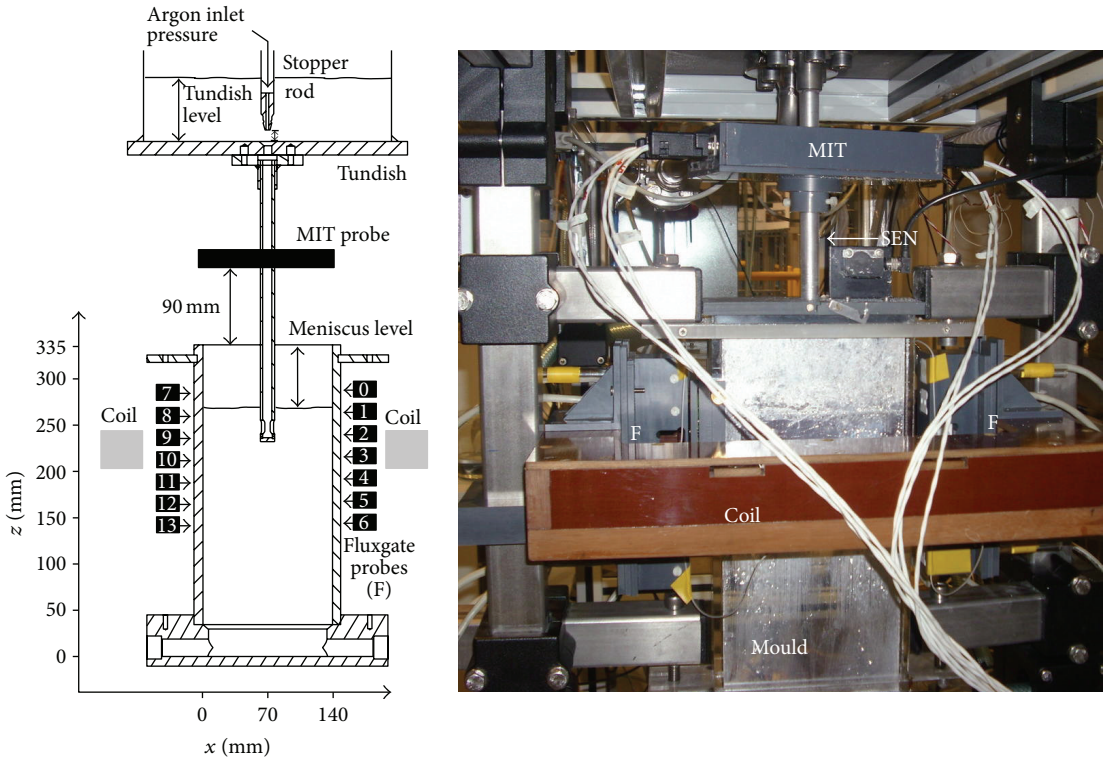


FIGURE 2: Application of CIFT to a flow problem related to the continuous casting of steel. Experimental set-up: a liquid metal (GaInSn) is poured through a submerged entry nozzle (SEN) into the mould with a rectangular cross-section of $140 \times 35\,\text{mm}^2$ and a height of 335 mm. Added Argon gas leads to a highly chaotic flow in the mould. A magnetic field of about 2 mT is applied by a coil. The flow induced magnetic fields are measured with $2 \times 7$ fluxgate sensors at the narrow faces of the mould.

The parameters $\sigma_{B_{0,k}}$ are the a priori errors for the measured induced magnetic fields. $\sigma_{\text{div}}$ is chosen very small in order to ensure the divergence-free condition. The parameter to play with in the regularization procedure is $\sigma_{\text{pen}}$. Here we employ the so-called Tikhonov regularization [3]: by increasing the regularization parameter $\sigma_{\text{pen}}^2$, one obtains solutions of the inverse problem with increasing kinetic energy of the flow. The optimal solution is then found at the point of strongest curvature of Tikhonov's L-curve which is done by an automatic search described in [18].

The above equation system is valid for the case of different applied magnetic fields and a fully three-dimensional flow. It can, however, also be adapted to the essentially two-dimensional case of slab-casting, where only one (basically vertical) magnetic field $B_{0,z}$ is applied. In this case, the dimensional reduction of the velocity structure from 3D to 2D can be realized by adding an additional functional

$$F_{\text{2D}}[\mathbf{v}] = \frac{1}{\sigma_{\text{2D}}^2} \sum_{l=1}^{n_V} v_{y,l}^2, \tag{11}$$

which enforces the velocity to be two dimensional by setting to zero the component $v_y$ (which is parallel to the narrow faces of the mould). Optionally, the mean velocity at some inlet points $l \in M_{\text{inlet}}$ can be prescribed by the functional

$$F_{v_{\text{inlet}}}[\mathbf{v}] = \frac{1}{\sigma_{v_{\text{inlet}}}^2} \sum_{l \in M_{\text{inlet}}} \left\{\mathbf{v}_l - \mathbf{v}_{l,\text{inlet}}\right\}^2. \tag{12}$$

It should be noted that regularization based on some reasonable norm of the velocity is actually more than only a trick since in most cases the assumption of a rather smooth velocity field is sensible from a physical point of view. For the same reason it is clear, however, that the method is not suited to detect very small vortices in a strongly turbulent flow (see [7, 8] for the corresponding uniqueness problem).

## 3. A Three-Dimensional Flow Reconstruction Problem

The first demonstration experiment [1] for CIFT aimed at reconstructing a propeller-driven three-dimensional flow of a liquid metal in a compact cylindrical vessel (see Figure 1(a)). We used 4.4 L of the eutectic alloy GaInSn which is liquid at room temperature. The flow was produced by a motor-driven propeller with a diameter of 6 cm inside a cylindrical polypropylene vessel with radius $R = 9$ cm. The height of the liquid metal is 17.2 cm, yielding an aspect ratio close to 1.

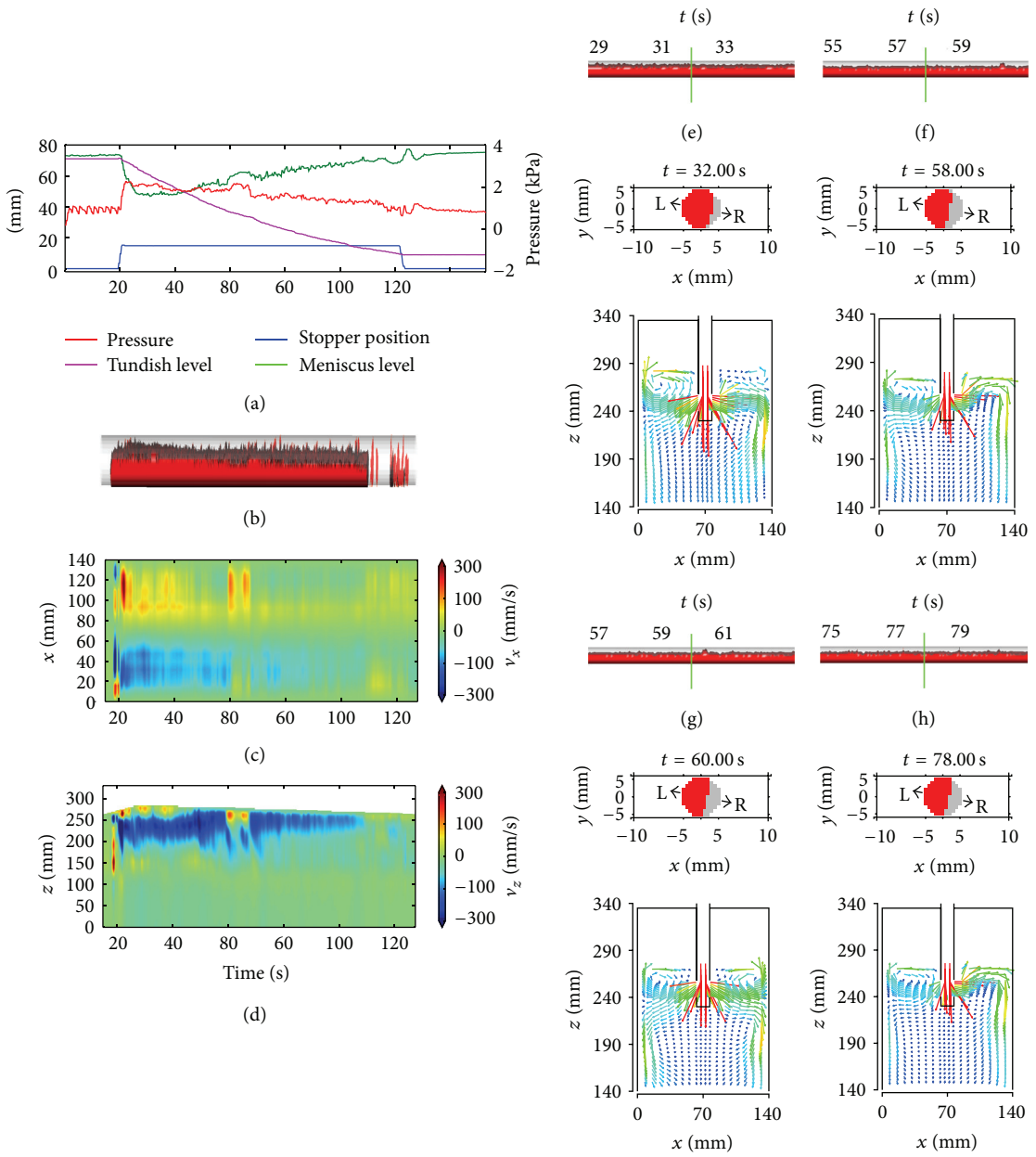


FIGURE 3: Results of MIT and CIFT for a test with an Argon flow rate of 400 $cm^3$/min: (a) pressure, stopper rod position, and tundish and meniscus level during the test; (b) spatial distribution of liquid metal (red) and Argon (gray) in the SEN in dependence of time; (c) CIFT-determined $v_x(t, x, z = 240\,\text{mm})$, (d) $v_z(t, z, x = 133\,\text{mm})$, and (e)–(h) snapshots of the MIT-determined liquid metal/Argon distribution in the SEN and of the CIFT-determined velocity field in the mould. Different flow structures are clearly visible. L and R denote the left and right port of the SEN, respectively.

For determining both the poloidal flow (in radial and axial direction) and the toroidal flow (in azimuthal direction), we applied subsequently a vertical $B_{0,z}$ and a horizontal $B_{0,x}$ magnetic field, both produced by Helmholtz-like coil pairs. The switching between the two fields occurs every 3 seconds, so that after 6 seconds all the magnetic field information was available for the velocity reconstruction. Admittedly, this is a rather poor time resolution, which can be significantly enhanced, with a physical limitation given by the magnetic decay time $\mu_0 \sigma R^2$, which is in the order of 0.05 s for the demonstration experiment.

For each of the two applied fields, $B_{0,z}$ and $B_{0,x}$, the components of the induced fields normal to the surface were measured at 48 positions, which are rather homogeneously distributed all over the surface of the cylindrical vessel. For the measurement we have used KSY 44 Hall sensors (Infineon) with an open-circuit sensitivity of around 200 V/AT. The rather small ratio of around $10^{-3} \cdots 10^{-2}$ between the

induced and the applied fields demands for a very stable current source of the Helmholtz-like coils, for a very stable relative position of Hall sensors and coils, and for significant effort to compensate drift and sensitivity changes of the Hall sensors (e.g., due to varying temperature).

By inverting the measured induced magnetic field data by the method described in the previous section, it was possible to distinguish clearly between upward and downward pumping of the propeller, with the rotational component being reduced by guiding blades in the case of upward pumping. For upward pumping, Figures 1(b) and 1(c) show the measured induced fields for applied $B_{0,z}$ and $B_{0,x}$, respectively, and Figure 1(d) depicts the velocity field as reconstructed from these two sets of information. The comparison with UDV measurements has shown a good coincidence of the resulting velocity fields [1]. Later, an additional confirmation of the flow was provided by Lorentz force velocimetry (LFV) measurements [19].

## 4. Dimensional Reduction: Application to Slab Casting Problems

In the continuous casting of steel slabs, the liquid metal flows from a tundish through a submerged entry nozzle (SEN), with typically two sideward directed ports at the lower end, into the mould where it starts to solidify at the water cooled copper walls. The flow structure in the mould plays a key role for the quality of the produced steel [20, 21]. Most desirable is a stable double-roll flow structure in which the two jets emanating from the SEN ports first reach the narrow-faces of the mould and then split into upward and downward directed branches. In contrast to that, the so-called single-roll structure, with the jets being sharply bent upward after leaving the SEN ports, is considered dangerous since it could lead to entrainment of casting powder into the steel. Any sort of online-monitoring of the detailed flow-structure in the mould could allow for an active control of the casting process, with the prospect to increase the possible casting speed significantly. As a contactless method, CIFT suggests itself for such monitoring, although the problem of the copper-mould oscillations makes its implementation in the industry still a formidable task.

As a first step in this direction, we have installed a simplified CIFT system at the small continuous casting model Mini-LIMMCAST, working also with the GaInSn alloy (Figure 2). The simplification concerns the restriction of the CIFT system to a single magnetic field coil which produces a mainly vertical magnetic field. This configuration is sufficient for the determination of the velocity component parallel to the wide faces of the mould [9], which is indeed the dominant one for the particular case of slab-casting. The induced fields are measured by fluxgate sensors positioned at the narrow faces of the mould, typically at 7 positions on either side. In addition to CIFT, we have utilized a mutual inductance tomography (MIT) system for determining the conductivity distribution in the SEN, which allows visualizing the details of the two-phase GaInSn/Argon flow [10, 13]. The simultaneous utilization of CIFT and MIT leads to a detailed understanding of the two-phase flow in the SEN and of the resulting flow in the mould. Figure 3 illustrates various flow structures that had been detected during one run of the experiment, including double-roll and single-roll structures occurring on different sides of the mould.

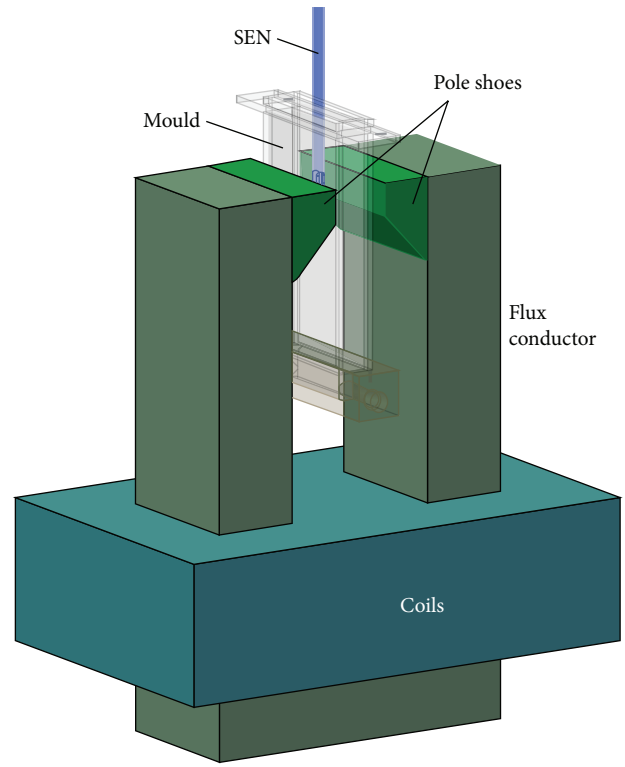


Figure 4: The central part of the Mini-LIMMCAST facility with an installed electromagnetic brake (EMBr).

## 5. Going to the Limits: CIFT in the Presence of a Strong Electromagnetic Brake

In the following we will show that CIFT is able to work even under the extreme condition that a strong static magnetic field is applied in addition to the measuring field. In continuous casting such strong fields are frequently used as electromagnetic brakes (EMBr) in order to influence the flow in the mould, and a lot of work is devoted to investigate their mode of operation and efficiency [22, 23].

Again, the experiments were conducted at the Mini-LIMMCAST slab caster model. This time, however, the induced magnetic fields were measured with $2 \times 7$ cylindrical induction coils positioned at the narrow faces of the caster model (the presence of the strong field prohibits the use of fluxgate sensors which would saturate approximately at 2 mT). Each induction coil has 340,000 windings with a conductor diameter of 25 $\mu$m. The signals from the coils were amplified by 20 dB using differential amplifiers made by FEMTO before being digitalized by an AdWin 18-bit-analog-digital-converter system. Since the induction coils pick up the superposition of the excitation field and the induced field, it is crucial to have a highly linear signal processing system.

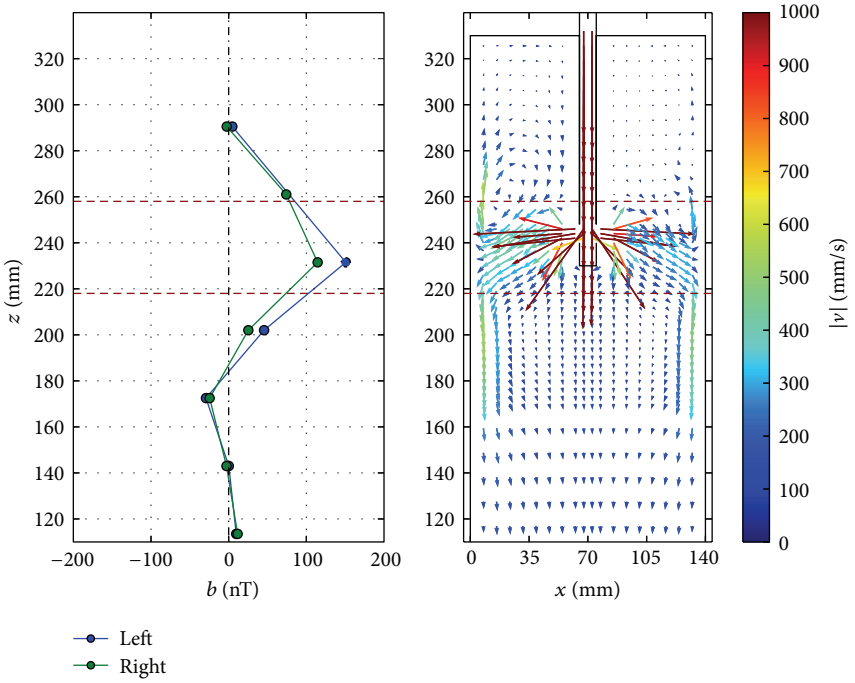


FIGURE 5: Left: snapshot of the measured induced magnetic fields at 14 induction coil positions on both narrow faces of the mould. Right: CIFT-reconstructed velocity field in the presence of pole shoes, but with the brake field being switched off. The position of the pole faces is indicated by the brown dashed lines.

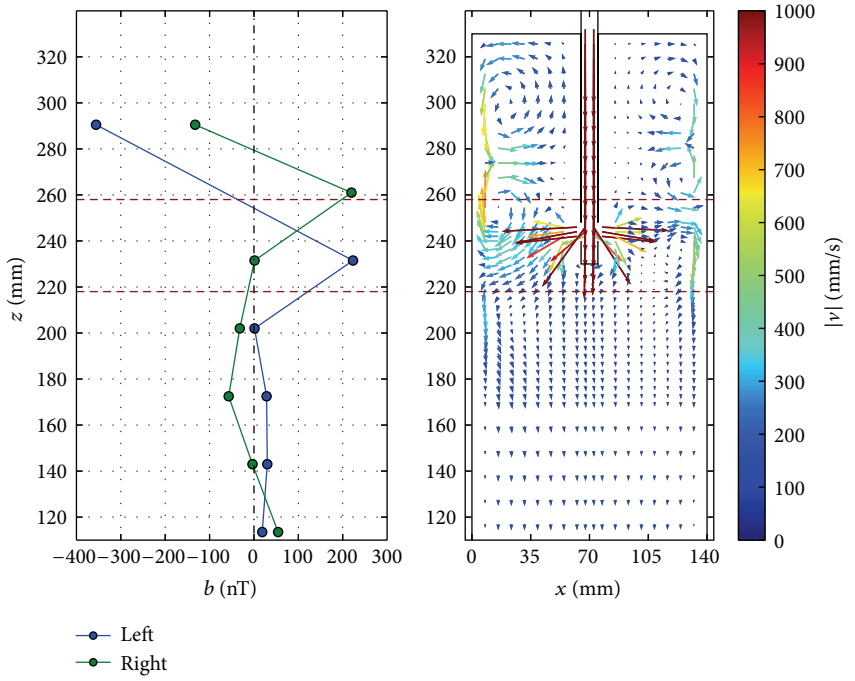


FIGURE 6: Same as Figure 5, but with a brake field of 300 mT being switched on.

A ruler-type brake was used to generate a DC magnetic field perpendicular to the wide faces of the mould and hence to the main flow direction (Figure 4). At first, Figure 5 shows a snapshot of the measured magnetic fields at 2 × 7 positions and the reconstructed velocity with the brake field being switched off. The obtained velocity field represents the rather stable double vortex flow which is well known from previous work [10]. Note, however, that the velocity reconstruction is

already quite complicated, since the significant deformation of the measuring field in the presence of the magnetic pole shoes must be taken into account.

Figure 6 shows then the measured induced fields and the reconstructed velocity for the case that the brake field is switched on. Our reconstruction shows that the average position of the jet has shifted upward, and that the return flow appears now closer to the jet, even forming a third vortex at the top of the mould. We also confirm the observations of [23] that the magnetic brake, contrary to previous expectations, leads to stronger fluctuations.

While more detailed investigations of these effects are still necessary, it is quite remarkable that on the background of a strong brake field of 300 mT it is possible to measure safely the induced magnetic fields which are 6-7 orders of magnitude smaller and to reconstruct from them the velocity.

## 6. Conclusions and Prospects

In this paper, we have surveyed the basic ideas and some first applications of CIFT. Presently, work is going on to further improve the robustness and the signal-to-noise ratio under the harsh mechanical and electromagnetic conditions that would prevail, for example, in a real casting plant. The key role is played here by the use of AC excitation with a low frequency, which allows for filtering out environmental noise, and by employing gradiometric probes with a similar effect. The use of AC fields with different frequencies could further allow, at least in principle, for a better resolution in the depth of the fluid by utilizing the different skin depths.

A main challenge for applying CIFT in a real steel caster is certainly the up-and-down oscillation of the copper mould. Even if the measuring coil, together with the sensors, could be stably installed at the mould, one has to be aware of disturbing induction effects due to the relative motion of the mould to the rest of the facility.

Another possible application field of CIFT may be the Czochralski crystal growth of silicon. First tests have already been made at various pullers. The main problem here is the comparably large distance between the silicon melt to be monitored and the sensor positions outside the vessel. While some artificially strong flow variations, for example, a change of the rotation direction of the quartz crucible with a subsequent slow adaptation of the melt flow, were already successfully identified by CIFT, a more detailed reconstruction of the flow structure still seems to be beyond the limits of CIFT. On the laboratory scale, CIFT-like flow inference methods have also been used in connection with the identification of current-driven instabilities [24] and with the flow reconstruction in Rayleigh-Benard cells with liquid metal.

A most interesting but ambitious project would be to combine into one single scheme the CIFT method with the mutual inductance tomography (MIT) [4, 5]. A simultaneous but yet spatially separated application of both methods at the Mini-LIMMCAST facility was already documented in [13]. The question is whether both conductivity variation and the velocity field could be obtained by one single measurement system. A first step in this direction was the reformulation of CIFT in terms of the sensitivity matrix [25].

## Conflict of Interests

The authors declare that there is no conflict of interests regarding the publication of this paper.

## Acknowledgments

This work was supported by Helmholtz-Gemeinschaft Deutscher Forschungszentren (HGF) in frame of the Helmholtz Alliance LIMTECH. The authors thank Konrad Klotsche and Klaus Timmel for technical support.

## References

[1] F. Stefani, T. Gundrum, and G. Gerbeth, "Contactless inductive flow tomography," *Physical Review E: Statistical, Nonlinear, and Soft Matter Physics*, vol. 70, Article ID 056306, 2004.

[2] M. Hämäläinen, R. Hari, R. J. Ilmoniemi, J. Knuutila, and O. V. Lounasmaa, "Magnetoencephalography—theory, instrumentation, and applications to noninvasive studies of the working human brain," *Reviews of Modern Physics*, vol. 65, no. 2, pp. 413–497, 1993.

[3] P. C. Hansen, "Analysis of discrete ill-posed problems by means of the *L*-curve," *SIAM Review*, vol. 34, no. 4, pp. 561–580, 1992.

[4] M. Soleimani, W. R. B. Lionheart, and A. J. Peyton, "Image reconstruction for high-contrast conductivity imaging in mutual induction tomography for industrial applications," *IEEE Transactions on Instrumentation and Measurement*, vol. 56, no. 5, pp. 2024–2032, 2007.

[5] X. Ma, A. J. Peyton, S. R. Higson, and P. Drake, "Development of multiple frequency electromagnetic induction systems for steel flow visualization," *Measurement Science and Technology*, vol. 19, no. 9, Article ID 094008, 2008.

[6] F. Stefani and G. Gerbeth, "Velocity reconstruction in conducting fluids from magnetic field and electric potential measurements," *Inverse Problems*, vol. 15, no. 3, pp. 771–786, 1999.

[7] F. Stefani and G. Gerbeth, "On the uniqueness of velocity reconstruction in conducting fluids from measurements of induced electromagnetic fields," *Inverse Problems*, vol. 16, no. 1, pp. 1–9, 2000.

[8] F. Stefani and G. Gerbeth, "A contactless method for velocity reconstruction in electrically conducting fluids," *Measurement Science and Technology*, vol. 11, no. 6, pp. 758–765, 2000.

[9] T. Wondrak, V. Galindo, G. Gerbeth, T. Gundrum, F. Stefani, and K. Timmel, "Contactless inductive flow tomography for a model of continuous steel casting," *Measurement Science and Technology*, vol. 21, no. 4, Article ID 045402, 2010.

[10] T. Wondrak, S. Eckert, G. Gerbeth et al., "Combined electromagnetic tomography for determining two-phase flow characteristics in the submerged entry nozzle and in the mold of a continuous casting model," *Metallurgical and Materials Transactions B: Process Metallurgy and Materials Processing Science*, vol. 42, no. 6, pp. 1201–1210, 2011.

[11] T. Wondrak, S. Eckert, V. Galindo et al., "Liquid metal experiments with swirling flow submerged entry nozzle," *Ironmaking and Steelmaking*, vol. 39, no. 1, pp. 1–9, 2012.

[12] K. Timmel, S. Eckert, G. Gerbeth, F. Stefani, and T. Wondrak, "Experimental modeling of the continuous casting process of steel using low melting point metal alloys-the LIMMCAST program," *ISIJ International*, vol. 50, no. 8, pp. 1134–1141, 2010.

[13] N. Terzija, W. Yin, G. Gerbeth et al., "Electromagnetic inspection of a two-phase flow of GaInSn and argon," *Flow Measurement and Instrumentation*, vol. 22, no. 1, pp. 10–16, 2011.

[14] F. Stefani, G. Gerbeth, and K.-H. Rädler, "Steady dynamos in finite domains: an integral equation approach," *Astronomische Nachrichten*, vol. 321, no. 1, pp. 65–73, 2000.

[15] J. Baumgartl, A. Hubert, and G. Müller, "The use of magnetohydrodynamic effects to investigate fluid flow in electrically conducting melts," *Physics of Fluids A*, vol. 5, no. 12, pp. 3280–3289, 1992.

[16] D. V. Berkov and N. L. Gorn, "Reconstruction of the velocity distribution in conducting melts from induced magnetic field measurements," *Computer Physics Communications*, vol. 86, no. 3, pp. 255–263, 1995.

[17] M. Xu, F. Stefani, and G. Gerbeth, "The integral equation method for a steady kinematic dynamo problem," *Journal of Computational Physics*, vol. 196, no. 1, pp. 102–125, 2004.

[18] T. Wondrak, F. Stefani, T. Gundrum, and G. Gerbeth, "Some methodological improvements of the contactless inductive flow tomography," *International Journal of Applied Electromagnetics and Mechanics*, vol. 30, no. 3-4, pp. 255–264, 2009.

[19] C. Heinicke and T. Wondrak, "Spatial and temporal resolution of a local Lorentz force flowmeter," *Measurement Science and Technology*, vol. 25, no. 5, Article ID 055302, 2014.

[20] S. Kunstreich and P. H. Dauby, "Effect of liquid steel flow pattern on slab quality and the need for dynamic electromagnetic control in the mould," *Ironmaking and Steelmaking*, vol. 32, no. 1, pp. 80–86, 2005.

[21] L. Zhang, S. Yang, K. Cai, J. Li, X. Wan, and B. G. Thomas, "Investigation of fluid flow and steel cleanliness in the continuous casting strand," *Metallurgical and Materials Transactions B: Process Metallurgy and Materials Processing Science*, vol. 38, no. 1, pp. 63–83, 2007.

[22] K. Cukierski and B. G. Thomas, "Flow control with local electromagnetic braking in continuous casting of steel slabs," *Metallurgical and Materials Transactions B*, vol. 39, no. 1, pp. 94–107, 2008.

[23] K. Timmel, S. Eckert, and G. Gerbeth, "Experimental investigation of the flow in a continuous-casting mold under the influence of a transverse, direct current magnetic field," *Metallurgical and Materials Transactions B*, vol. 42, no. 1, pp. 68–80, 2011.

[24] M. Seilmayer, F. Stefani, T. Gundrum et al., "Experimental evidence for a transient Tayler instability in a cylindrical liquid-metal column," *Physical Review Letters*, vol. 108, no. 24, Article ID 244501, 2012.

[25] W. Yin, A. J. Peyton, F. Stefani, and G. Gerbeth, "Theoretical and numerical approaches to the forward problem and sensitivity calculation of a novel contactless inductive flow tomography (CIFT)," *Measurement Science and Technology*, vol. 20, no. 10, Article ID 105503, 2009.



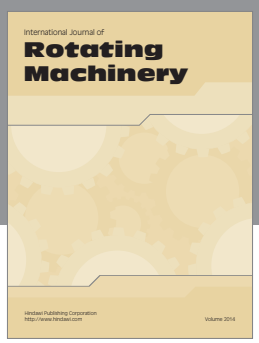




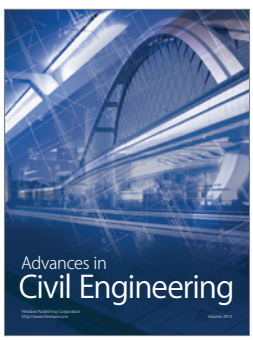


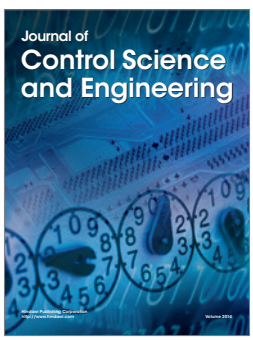



Hindawi
Submit your manuscripts at
http://www.hindawi.com